

The Intraseasonal Oscillation of Eastern Tibetan Plateau Precipitation in Response to the Summer Eurasian Wave Train

WENTING HU AND ANMIN DUAN

*State Key Laboratory of Numerical Modeling for Atmospheric Sciences and Geophysical Fluid Dynamics (LASG),
Institute of Atmospheric Physics, Chinese Academy of Sciences, Beijing, China*

YUN LI

Western Power Business Intelligence and Data Analytics, Perth, Australia

BIAN HE

*State Key Laboratory of Numerical Modeling for Atmospheric Sciences and Geophysical Fluid Dynamics (LASG),
Institute of Atmospheric Physics, Chinese Academy of Sciences, Beijing, China*

(Manuscript received 31 August 2015, in final form 15 July 2016)

ABSTRACT


This study examines the characteristics and mechanisms associated with the dominant intraseasonal oscillation (ISO) that controlled eastern Tibetan Plateau summer rainfall (ETPSR) over the period 1979–2011. The results of both power and wavelet spectrum analysis reveal that ETPSR follows a significant 7–20-day oscillation during most summers. The vertical structure of the ETPSR ISO in the dry phase is characterized by a vertical dipole pattern of geopotential height with a positive center on the eastern Tibetan Plateau (TP) and a negative center on the western TP. The wet phase shows the opposite characteristics to the dry phase. The transitions between the dry and wet phases during an ETPSR ISO cycle are related to a Rossby wave train that presents as large anomalous anticyclonic and cyclonic centers that alternate along the pathway from the eastern Atlantic to southern China via the TP. It corresponds to the evolution of the phase-independent wave-activity \mathbf{W} , which implies an eastward/southeastward energy propagation of the ISO. The dominant modes of the daily 200-hPa geopotential height as identified by the rotated empirical orthogonal function (REOF) demonstrate that the different phases of the Rossby wave train influence the upper-level circulation over the eastern TP, which then impacts precipitation in the region. Furthermore, fluctuations in the eastern Atlantic may be the key factor for the propagation of the Rossby wave train that influences the upper-level circulation and rainfall variability over the eastern TP. Results from numerical experiments using an atmospheric general circulation model support the conclusion that the fluctuations over the eastern Atlantic contribute to the ISO of ETPSR.

1. Introduction

Since a 40–50-day eastward-propagating oscillation in the tropics during the boreal winter was discovered by [Madden and Julian \(1971, 1972\)](#), the study of intraseasonal oscillations (ISOs) has been extended to the

boreal summer and extratropics. The related characteristics and mechanisms have been well documented in many studies (e.g., [Goswami 2005](#); [Waliser 2005, 2006](#)).

During the boreal summer, the monsoon ISO displays more complicated characteristics than the Madden–Julian oscillation (MJO), with both eastward and northward propagation (e.g., [Yasunari 1979, 1980, 1981](#); [Annamalai and Slingo 2001](#); [Lawrence and Webster 2002](#); [Jiang et al. 2004](#); [Hu et al. 2015](#)). Furthermore, ISOs are responsible for the rainfall variability that occurs in monsoon regions within the annual cycle, which has a significant impact on the local weather and climate (e.g., [Mao and Chan 2005](#); [Yang et al. 2008, 2010, 2014](#)). [Mao and Chan \(2005\)](#) explored the intraseasonal variability of the South China

 Denotes Open Access content.

Corresponding author address: Dr. Wenting Hu, State Key Laboratory of Numerical Modeling for Atmospheric Sciences and Geophysical Fluid Dynamics (LASG), Institute of Atmospheric Physics, Chinese Academy of Sciences, Beijing 100029, China.
E-mail: hwt@lasg.iap.ac.cn

DOI: 10.1175/JCLI-D-15-0620.1

Sea (SCS) summer monsoon in terms of its structure and propagation, and suggested that the 10–20-day oscillation manifests as an anticyclone–cyclone system over the western tropical Pacific before moving northwestward into the SCS. Two dominant intraseasonal variations over the lower reaches of the Yangtze River basin during the boreal summer were identified by Yang et al. (2010), with spectral peaks at around 15 and 24 days.

In addition, the characteristics of extratropical ISOs over or around the Tibetan Plateau (TP) differ from the tropical oscillations in terms of periodicity and propagation. Murakami (1981) analyzed those ISOs with a period of 12–20 days on the Asian subtropical jet over and around the TP during the northern winter, and found that the topography of the TP profoundly influences the formation, propagation, and dissipation of this oscillation. Fujinami and Yasunari (2001) reported fluctuations in the diurnal amplitude of summertime convection with periods of about 14 and 30 days over the TP. Using data for three years (1986, 1993, and 1998), Fujinami and Yasunari (2004) examined convective variability over submonthly time scales (7–20 days) on the TP and the associated large-scale atmospheric circulation. They suggested that the 7–20-day convective variability over the TP is associated with a wave train propagating from North Africa to Japan along the Asian subtropical jet. Furthermore, Fujinami and Yasunari (2009) pointed out that two contrasting patterns of Rossby wave trains along the Asian jet greatly influence the convective variability over submonthly time scales (7–25 days) in the Yangtze and Huaihe River basins during the mei-yu season. At the synoptic time scale, the propagation or break of upper-tropospheric Rossby waves has a major impact on moisture transport and precipitation over summertime East Asia and the northwestern Pacific (Horinouchi 2014). Park et al. (2015) also found that the extratropical wave train over the Eurasian continent has a significant influence on the southerly wind and rainfall variability over eastern China.

Although these studies demonstrated that the intraseasonal variability of climate systems over or around the TP is related to the Rossby wave train along the Asian subtropical jet, their results did not reveal the coupling mechanisms over intraseasonal scales between the Rossby wave train and rainfall variability on the TP, and this was because of limitations in the datasets used. However, further consideration of long-term daily rain gauge observations will allow us to address several of the major questions that remain from these previous studies, as follows. 1) What are the dominant intraseasonal modes that controlled eastern TP summer rainfall (ETPSR) activity in the 33 summers from 1979 to 2011? 2) How does the intraseasonal Rossby wave train influence the

rainfall variability over the eastern TP (ETP)? 3) What influences the propagation of the wave train that is related to the ETPSR ISO? We aim to answer these questions through both observational analysis and sensitivity experiments using an atmospheric general circulation model (AGCM).

In the remainder of the paper, section 2 describes the data, methods, and model used in this study; the dominant periodicity, temporal evolution, and vertical structure of the ETPSR ISO are analyzed in section 3; the teleconnection between the summer Eurasian wave train and the ETPSR ISO is investigated in section 4; and the impact of fluctuations over the eastern Atlantic on ETPSR is examined in section 5. Finally, a summary and discussion are presented in section 6.

2. Data, methods, and model

a. Data

Daily rain gauge observations at 69 stations on the ETP (25° – 40° N, 85° – 105° E), with temporal continuity and no missing values for the summer period of June–August (JJA) between 1979 and 2011, were selected from the 756 stations in China. These data were provided by the National Meteorological Information Center of the China Meteorological Administration (CMA). Quality control procedures were applied to the station data to eliminate erroneous data and ensure homogeneity. The locations of the 69 stations on the ETP are shown in Fig. 1. Note that because of the lack of data over the western TP (only three stations west of 85° E) we focus here on the characteristics of intraseasonal variability of ETPSR, rather than across the whole TP.

Daily mean wind, vertical velocity, temperature, and geopotential height from both the National Centers for Environmental Prediction (NCEP)–U.S. Department of Energy (DOE) Reanalysis 2 (Kanamitsu et al. 2002) and the European Centre for Medium-Range Weather Forecasts (ECMWF) interim reanalysis (ERA-Interim; Dee et al. 2011) datasets were used to examine the atmospheric horizontal circulation and vertical structure. As the two datasets generate similar results, for ease of presentation here we provide only the results from the NCEP–DOE Reanalysis 2 dataset, with a horizontal resolution of $2.5^{\circ} \times 2.5^{\circ}$. The period of analysis covered the 33 summers between 1979 and 2011.

b. Methods

A two-step temporal filtering scheme that aims to preserve intraseasonal variability was applied to the daily data to remove long-term variability as follows. First, the climatological daily mean for the period JJA is

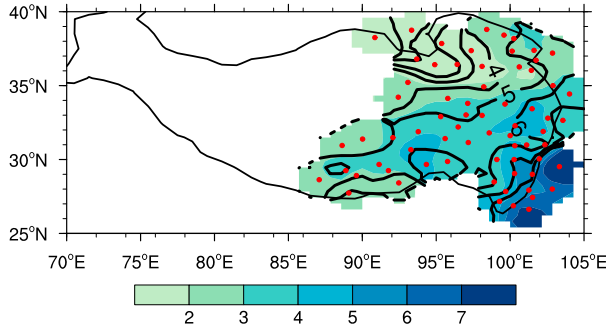


FIG. 1. Spatial pattern of climatological summer (JJA) daily precipitation (shading; mm day^{-1}) and its standard deviation (contours) over the ETP for the period 1979–2011. Red dots represent the locations of the 69 stations used in the study. The TP with terrain above 3000 m is outlined by the solid thin black curve.

removed from the raw data to eliminate the climatological seasonal cycle. A 5-day running mean is then calculated to remove synoptic fluctuations. Except for first examining the climatological pattern of JJA precipitation and its standard deviation over the ETP (Fig. 1), all variables used in this study were processed according to this two-step procedure prior to subsequent analysis.

To represent the evolution of ETPSR, the average of the selected 69 stations was chosen as a reference time series, and will be referred to as the ETPSR index (ETPSRI) for simplicity. Power spectrum analysis (Gilman et al. 1963) was applied to the ETPSRI during each summer to identify the dominant periodicity. Mean power spectrum and wavelet spectrum were calculated by taking the average of the individual power/wavelet spectra for the 33 summer seasons from 1979 to 2011 to

obtain the common periodicity. The ISO signals were extracted from the daily data using a Lanczos bandpass filter (Duchon 1979), which has the significant advantage of reducing the Gibbs oscillation. The phase composite techniques (e.g., Mao and Chan 2005; Pan et al. 2013) were also used to analyze the ISO life cycle. In the present study, a Student's t test was used to examine the significance of the results. The effective degree of freedom ν for the significance test was estimated as follows:

$$\nu = n \frac{1 - r_{1x}r_{1y}}{1 + r_{1x}r_{1y}}, \quad (1)$$

where n is the sample size, and r_{1x} and r_{1y} are the autocorrelations of the time series.

We investigated the dynamical process related to the ETPSR ISO through the wave activity flux. Takaya and Nakamura (2001) formulated a phase-independent wave activity flux \mathbf{W} for stationary and migratory quasigeostrophic eddies on a zonally varying basic flow. This is a useful diagnostic tool for obtaining a “snapshot” of a propagating packet of stationary or migratory quasigeostrophic wave disturbances and thereby inferring where the packet is emitted and absorbed (Takaya and Nakamura 2001). Compared with the approach of Plumb (1985), it can depict instantaneous three-dimensional wave packet propagation, derived without any averaging, which is its greatest advantage.

In spherical coordinates, \mathbf{W} may be expressed as follows:

$$\mathbf{W} = \frac{p \cos \phi}{2|\mathbf{U}|} \begin{pmatrix} \frac{U}{a^2 \cos^2 \phi} \left[\left(\frac{\partial \psi'}{\partial \lambda} \right)^2 - \psi' \frac{\partial^2 \psi'}{\partial \lambda^2} \right] + \frac{V}{a^2 \cos \phi} \left[\frac{\partial \psi'}{\partial \lambda} \frac{\partial \psi'}{\partial \phi} - \psi' \frac{\partial^2 \psi'}{\partial \lambda \partial \phi} \right] \\ \frac{U}{a^2 \cos \phi} \left[\frac{\partial \psi'}{\partial \lambda} \frac{\partial \psi'}{\partial \phi} - \psi' \frac{\partial^2 \psi'}{\partial \lambda \partial \phi} \right] + \frac{V}{a^2} \left[\left(\frac{\partial \psi'}{\partial \phi} \right)^2 - \psi' \frac{\partial^2 \psi'}{\partial \phi^2} \right] \\ \frac{f_0^2}{N^2} \left\{ \frac{U}{a \cos \phi} \left[\frac{\partial \psi'}{\partial \lambda} \frac{\partial \psi'}{\partial z} - \psi' \frac{\partial^2 \psi'}{\partial \lambda \partial z} \right] + \frac{V}{a} \left[\frac{\partial \psi'}{\partial \phi} \frac{\partial \psi'}{\partial z} - \psi' \frac{\partial^2 \psi'}{\partial \phi \partial z} \right] \right\} \end{pmatrix} + \mathbf{C}_U M, \quad (2)$$

where U and V are the zonal and meridional components of the basic flow, respectively; λ and ϕ are longitude and latitude, respectively; a is Earth's radius; f_0 is the Coriolis parameter; N^2 is the buoyancy frequency; and p is the pressure scaled by 1000 hPa. Considering small-amplitude perturbation on a steady zonal inhomogeneous basic flow $\psi = \Psi(x, y, z) + \psi'$, the three-dimensional perturbation streamfunction is denoted by ψ' .

The wave-activity (angular) pseudomomentum M is defined as

$$M = \frac{p}{2} \left(\frac{q'^2}{2|\nabla_H Q|} + \frac{e}{|\mathbf{U}| - C_p} \right) \cos \phi, \quad (3)$$

where q' and Q are the potential vorticity of the wave and basic flow, respectively; e is wave energy; ∇_H is a

horizontal Hamiltonian operator; C_p is the phase speed of migratory perturbation in the direction of the basic flow \mathbf{U} ; and \mathbf{C}_U represents the phase propagation vector in the direction of $\mathbf{U}(U, V)$. The detailed method used to calculate \mathbf{W} can be found in Takaya and Nakamura (2001) and Pan et al. (2013).

c. Model

The model used in this study was the LASG/IAP Spectral Atmospheric Model (known as SAMIL; Wu et al. 1996; Bao et al. 2013), which has a horizontal spectral resolution of R42 (2.81° longitude \times 1.66° latitude) and 26 vertical layers in sigma–pressure hybrid coordinates extending from the surface to 2.19 hPa. The mass flux cumulus parameterization of Tiedtke (1989) was used to calculate convective precipitation. The cloud scheme was a diagnostic method parameterized by low-layer static stability and relative humidity (Slingo 1980, 1989). A stratocumulus scheme based on a statistical cloud scheme (Dai et al. 2004) and a nonlocal scheme are used to calculate the eddy-diffusivity profile and turbulent velocity scale; the model also incorporates nonlocal transport effects for heat and moisture (Holtlag and Boville 1993). This model contains the Edwards–Slingo radiation scheme (Edwards and Slingo 1996), incorporating some of the improvements proposed by Sun (2011). SAMIL was coupled with the NCAR CLM3 land model (Oleson et al. 2004) in this study. Monthly SST and sea ice were prescribed according to the 20-yr climatology used by phase two of the Atmospheric Model Intercomparison Project (AMIP II; see http://www-pcmdi.llnl.gov/projects/amip/AMIP2EXPDSN/BCS_OBS/amip2_bcs.htm for details). These monthly mean conditions were linearly interpolated to each integration step.

3. Characteristics of the ETPSR ISO

a. Dominant periodicity

Our analysis begins with an examination of the climatological pattern of summer (JJA) precipitation and its standard deviation over the eastern TP for the period 1979–2011 (Fig. 1). Both the climatological and standard deviation fields increase from north to south. Note that the maximum rainfall (exceeding 7 mm day^{-1}) occurs over the southeast corner of the TP, and this may be closely related to orographic effects.

As ETPSRI reflects the daily time-varying amplitude over each summer, it was selected as the reference time series from which we identified the dominant ISO signals on the TP. Figures 2a–d show the normalized unfiltered daily ETPSRI (black lines) for 1986, 1989, 1993, and 2002. It is evident that there are intraseasonal

fluctuations with different amplitudes each summer. As shown by the power spectrum analysis (Figs. 2e–h), there are always two or three peaks in the power spectra from the selected year, and the periodicities also vary with the year. For a case study, each peak periodicity should be analyzed separately in a specific year; however, the purpose of the present study is to investigate the main characteristics of the ETPSR ISO over a common period. The 7–20-day band is the common oscillation period for the selected years (significant at the 95% confidence level). The corresponding 7–20-day-filtered ETPSRI (red lines in Figs. 2a–d) accurately depicts the temporal characteristics of the intraseasonal fluctuations. In particular, the 7–20-day oscillation accounts for 51.8% (1986), 75.5% (1989), 49.3% (1993), and 46.6% (2002) of the variance in the ISO signals of ETPSR (Figs. 2a–d). These results suggest that there is a year-to-year variability with the 7–20-day ISO features in the ETPSRI for 1986, 1989, 1993, and 2002. To confirm the 7–20-day ISO features of the ETPSRI in most years, we calculated the 33-summer averaged power spectrum and wavelet power spectrum from 1979 to 2011. As shown in Fig. 3, the 7–20-day band is statistically significant at the 95% confidence level, and the peak amplitude of the averaged power spectrum appears between 12 and 15 days. Therefore, the ETPSRI shows a significant 7–20-day oscillation in most summers over the study period.

In a future study, we will focus on the 7–20-day ISO of ETPSR, revealing its characteristics and associated driving processes.

b. Structure and evolution of the 7–20-day ETPSR ISO

To investigate the characteristics of the 7–20-day ETPSR ISO, the Lanczos filter was used to extract the 7–20-day ISO components from the ETPSRI and related three-dimensional meteorological variables of geopotential height, winds, vertical velocity, air temperature, and phase-independent wave-activity flux. Further, the phase composite analysis of the various fields was performed based on the definition of the different phases for ETPSRI to demonstrate the structure and evolution of the 7–20-day ETPSR oscillation.

Following Mao and Chan (2005) and Pan et al. (2013), strong ISO cycles are identified when the cycle includes both a wet and a dry period, with the peak magnitude of the wet or dry period exceeding a threshold of one standard deviation of daily filtered rainfall. According to this definition, there were 96 strong ISO cycles during the 33 summers between 1979 and 2011. As presented in Fig. 2a, each cycle is divided into eight phases. Phase 1 represents the dry period with the minimum value of

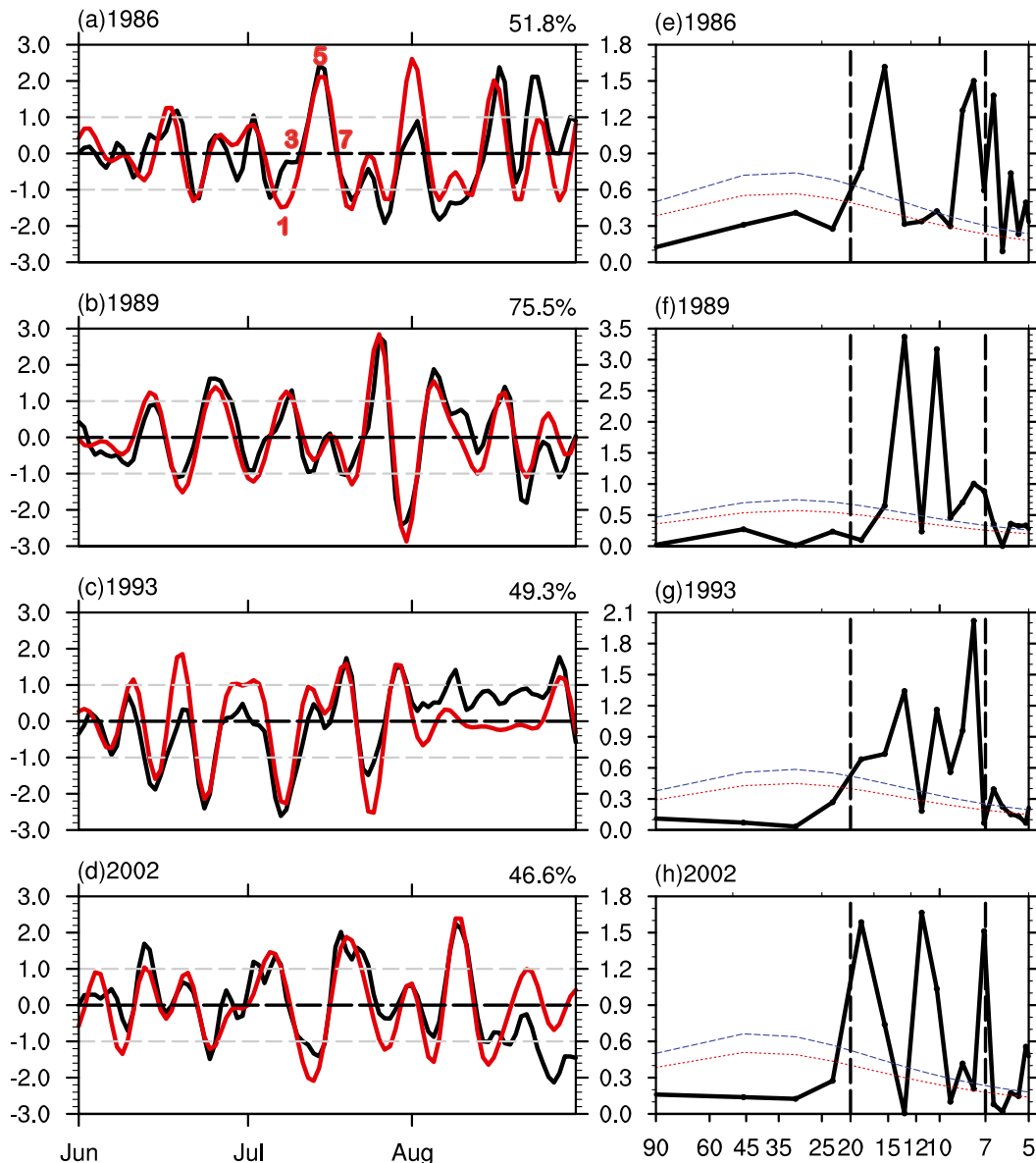


FIG. 2. Time series of normalized unfiltered (black line) and the 7–20-day-filtered (red line) ETPSRI for typical years (a) 1986, (b) 1989, (c) 1993, and (d) 2002. (e)–(h) The corresponding power spectra of the unfiltered area-averaged daily precipitation (black solid line), together with the Markov red noise spectrum (red dotted line) and a 95% confidence level (blue dashed line) for the selected years. The numbers 1, 3, 5, and 7 in (a) indicate the phases of one 7–20-day oscillation. The percentage variance of the 7–20-day oscillation in each selected year is marked on the top right of (a)–(d).

ETPSRI, whereas phase 5 corresponds to the wet period with a maximum value. Phases 3 and 7 are the transition periods. Phases 2 and 8 are defined as times when the oscillation reaches half of the minimum filtered ETPSRI, and phases 4 and 6 are times when the oscillation reaches half of the maximum filtered ETPSRI.

Figure 4 shows the composite evolution of the 7–20-day-filtered 200-hPa streamlines, divergence, and the horizontal components of the wave-activity flux \mathbf{W} in phases

1–8 of the 96 strong ISO cycles. In phase 1 (Fig. 4a), the upper-level circulations are characterized by a Rossby wave train with a series of enclosed anomalous anticyclonic (A1), cyclonic (C1), anticyclonic (A2), and cyclonic (C2) centers located over eastern Europe, central Asia, the central TP, and most of China, respectively, with strong divergence or convergence in between. The upper-level circulation in phase 2 (Fig. 4b) shows a splitting of the eastern European anticyclone (A1) into

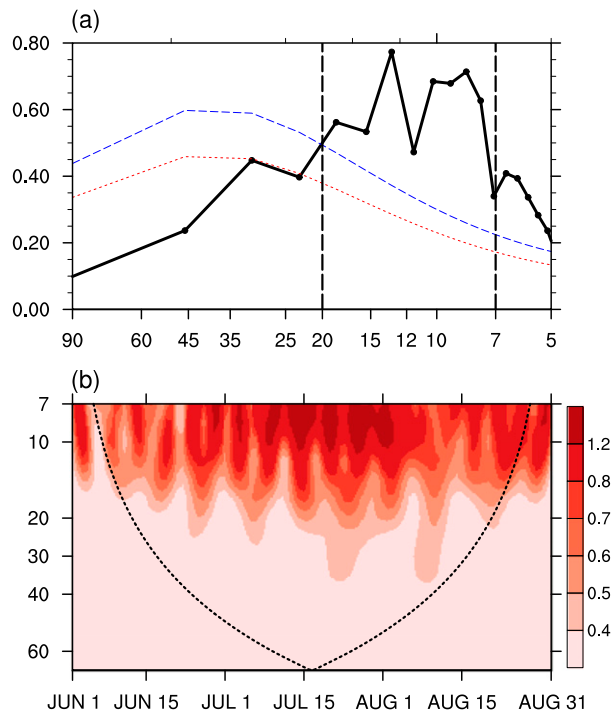


FIG. 3. The 33-summer averaged (a) power spectrum and (b) wavelet power spectrum of the unfiltered ETPSRI from 1979 to 2011. The red dotted and blue dashed lines in (a) represent the Markov red noise spectrum and a 95% confidence level, respectively. Dashed lines in (b) indicate the cone of influence outside of which edge effects become important (Torrence and Compo 1998).

two centers, with the southern one located over northern Africa, related to the intervention of the cyclonic branch (C4) from circumpolar latitudes. Meanwhile, the intensity of cyclones (C1 and C2) over central Asia and southern China decreases, in contrast to the elongated anticyclone A2 that strengthens and extends over the whole ETP and northern China. Note that there is a new anomalous cyclonic circulation (C3) located over the eastern Atlantic in phase 2. In phase 3 (Fig. 4c), corresponding to the southward movement of C4, the two centers of A1 weaken. The original weak cyclone (C1) intensifies, while the cyclone C2 over southern China has collapsed. As such, a wave train with alternate cyclonic and anticyclonic centers is generated, extending from the eastern Atlantic to the ETP. From phase 4 to 5 (Figs. 4d,e), the pair C3–A1 weakens and finally dissipates, while the intensities of C4, A1, C1, and A2 are increasing. Afterward, the divergence–anticyclone system weakens and moves to southern China, and then disappears in phase 6 (Fig. 4f). The divergence and circulation patterns of phase 7 (Fig. 4g) are the reverse of those of phase 3. The wave train continuously propagates eastward and southeastward (Fig. 4h), and then

another ISO cycle begins. Furthermore, the mainly eastward and southeastward propagations of the wave train during the ISO cycle can be supported by the wave-activity flux (\mathbf{W}) field. For instance, as indicated in Fig. 4, southeastward movement of \mathbf{W} from the Turan Plain to southern China occurs in all phases of the ISO cycle. Naoe et al. (1997) and Naoe and Matsuda (1998) examined the evolution of the propagating quasi-stationary Rossby wave using linear and nonlinear atmospheric models for idealized and realistic westerly waveguides. Their results showed that the Asian jet stream acts like a waveguide, and the propagation of the Rossby wave slows down near the jet exit, where the wave amplifies. This may explain why the amplitude of the wave-activity flux over East Asia is larger than that in other areas, and this is related to the barotropic conversion of kinetic energy (Naoe and Matsuda 1998).

The above analysis reveals that the evolution of the 7–20-day ISO of ETPSR is associated with the mainly eastward and southeastwards propagation of a wave train characterizing as large anomalous anticyclonic and cyclonic centers alternating along the pathway from eastern Atlantic to southern China via the TP in the upper-level troposphere. Specifically, in phase 1 (Fig. 4a), the wave train in the upper troposphere is associated with negative divergence anomalies over the ETP, western Asia, and western Europe, while positive divergence anomalies are found in southern China, the western TP, and eastern Europe. From phase 2 to phase 8 (Figs. 4b–h), the wave train displays a divergence pattern propagating eastward to the west of the TP and then moves southeastward from the western TP to southern China. During the wet phase (Fig. 4e), a strong divergence center is located over the ETP, corresponding to the maximum precipitation there. The composite evolution of moisture flux divergence vertically integrated from the surface to 100 hPa shows that there is also a moisture convergence center over the ETP during the wet phase (figures not shown). During the transitions between the dry and wet phases in an ETPSR ISO cycle, the moisture divergence pattern characterizes as a similar wave train propagating southeastward from eastern Europe to the ETP.

To further investigate the vertical structure of this wave train associated with the ETPSR ISO, we present pressure–longitude cross sections (Fig. 5) of composite 7–20-day-filtered airflow, geopotential height, and air temperature averaged over 35°–40°N during an ISO cycle. During the dry phase (Fig. 5a), there is a significant cool anomaly band extending from the lower troposphere over the western TP to the upper troposphere over the ETP. On the western edge of the TP, there is strong ascending motion between the negative and positive geopotential height centers. The convergence in

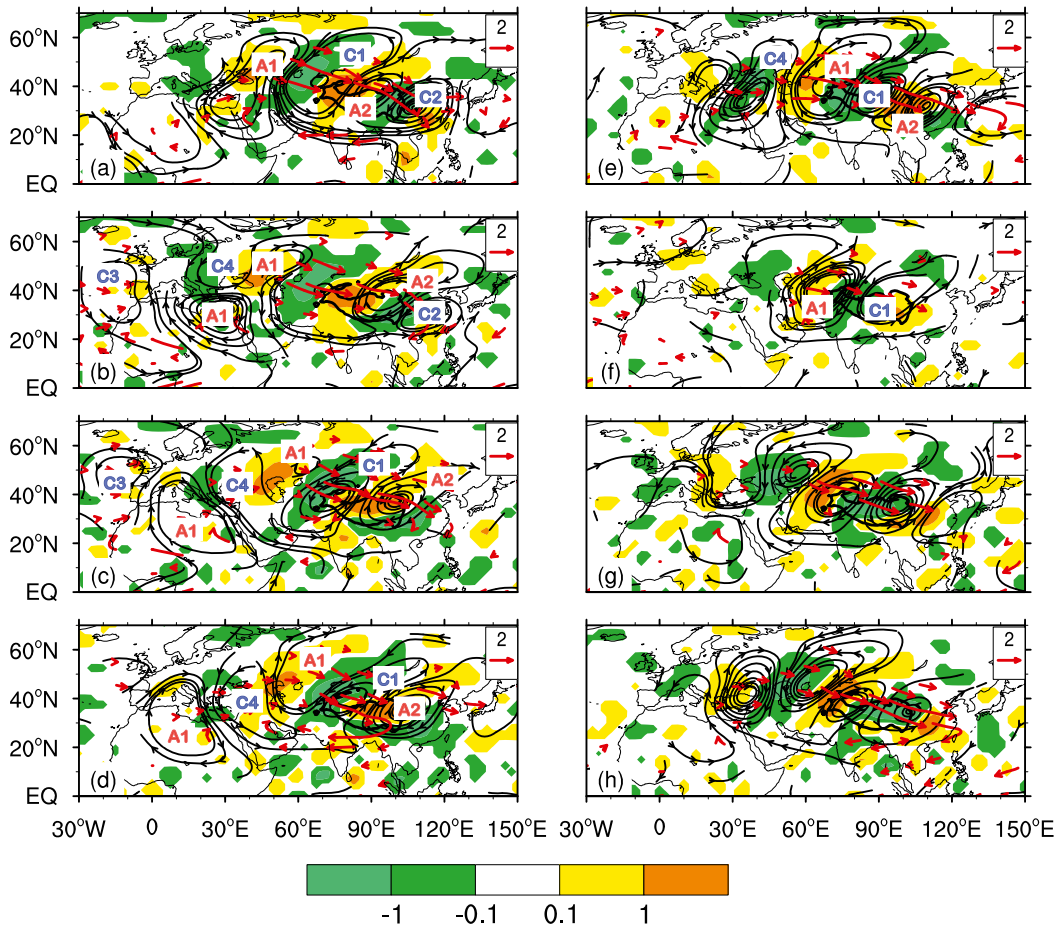


FIG. 4. Composite evolution of the 7–20-day-filtered 200-hPa streamline (where at least one wind component is statistically significant at the 90% confidence level), divergence (shading; 10^{-6} s^{-1} ; only shown if statistically significant at the 90% confidence level), and horizontal components of the wave-activity flux \mathbf{W} (vectors; $\text{m}^2 \text{ s}^{-2}$) during an ISO cycle, for (a)–(h) phases 1–8, respectively. The TP with terrain above 3000 m is outlined by the solid black curve. The notations with A and C indicate anticyclone and cyclone, respectively.

the upper-level troposphere over the ETP (Fig. 4a) induces descending motion there by continuity. The pair of geopotential height centers slowly propagates eastward from phase 2 to 4 (Figs. 5b–d) until the negative center is located on the ETP (Fig. 5e). At the same time, a new positive geopotential center is generated west of the TP (Fig. 5d), and moves together with the original negative center, forming a new pair of geopotential centers on the TP in phase 5 (Fig. 5e). The ascending motion leads to a large amount of rainfall over the ETP, corresponding to the wet phase. Then, this new pair of centers continues to move eastward. When the positive center occupies the ETP, which is unfavorable for ETPSR, the cycle is finished. This is consistent with the vertical structure of the extratropical wave train shown in Fig. 6 of Park et al. (2015). They also suggested that the upper-level wave propagation can affect the mid- and lower-tropospheric circulations by

changing static stability. The strengthening of ascending motion over the ETP during the wet phase may be induced by the reduced static stability as an initiating factor.

Another important feature related to the evolution of the 7–20-day ETPSR ISO is the fluctuation over the eastern Atlantic. When precipitation over the ETP is at a minimum, there is a weak negative geopotential height center with ascending motion below 300 hPa in the eastern Atlantic (Fig. 5a). In phase 2, the center over the eastern Atlantic extends to the upper-level troposphere and strengthens, while a positive geopotential height anomaly center appears at 150 hPa to its east (Fig. 5b). The intensity of these negative–positive–negative geopotential height centers between 30°W and 50°E increases in phase 3 (Fig. 5c). A new positive geopotential height center, which will have a great impact on ETPSR later, then forms at 60°E in phase 4 (Fig. 5d). The situation from the wet phase to phase 8 (Figs. 5e–h)

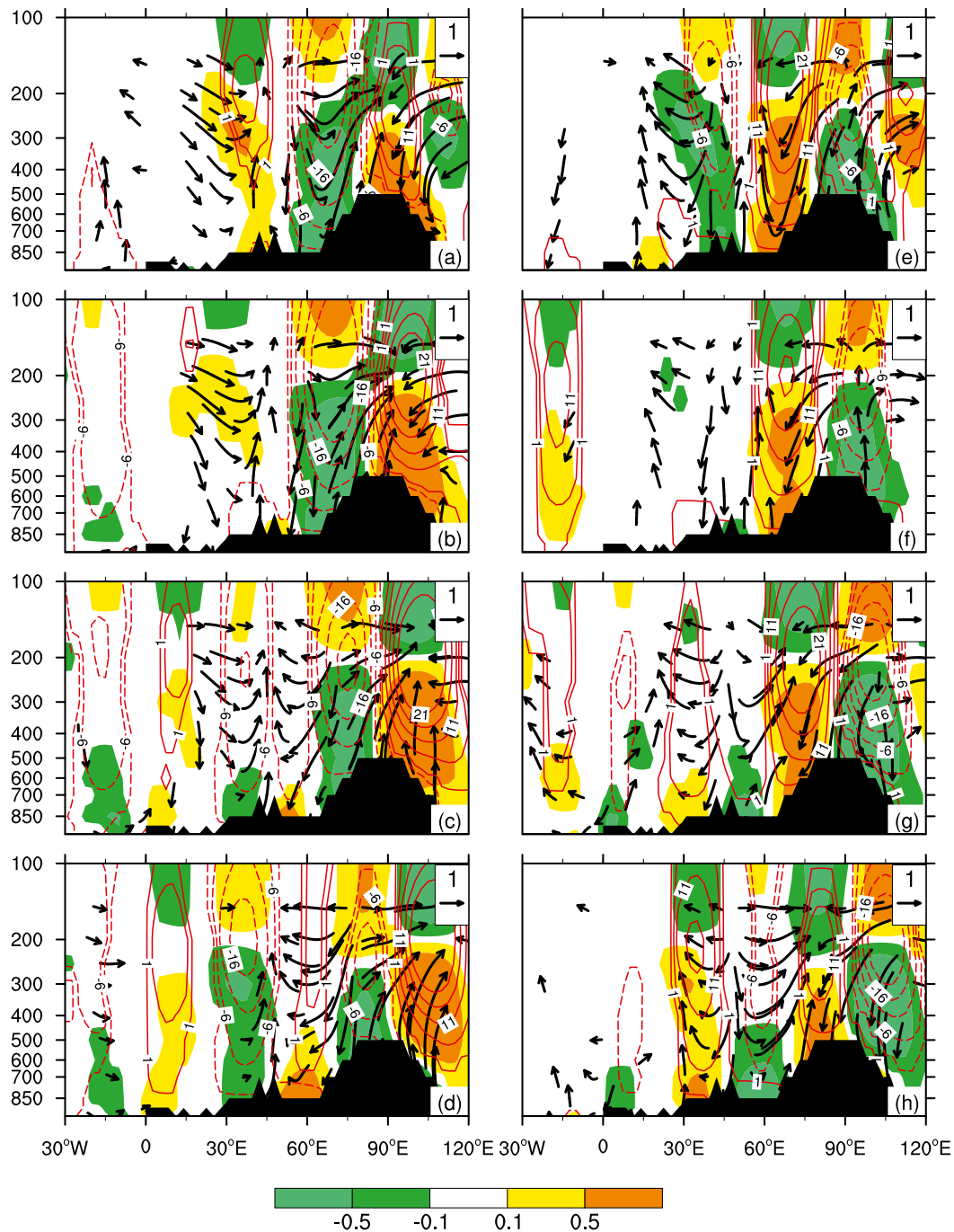


FIG. 5. The average 35° – 40° N pressure–longitude cross sections of composite 7–20-day-filtered airflow [vectors, u (m s^{-1}) and vertical velocity ($-200 \times \omega$; Pa s^{-1})], air temperature (shading; K), and geopotential height (contours every 5 gpm) during an ISO cycle for (a)–(h) phases 1–8, respectively. Only the values of winds (at least one component), geopotential height, and air temperature that are statistically significant at the 90% confidence level are plotted. The topography is shaded black.

is completely opposite to the previous half cycle. A positive geopotential height center with weak descending motion develops during the wet phase over the eastern Atlantic (Fig. 5e), which leads to the generation

of a series of negative–positive–negative geopotential height centers over Europe and central Asia (Figs. 5f–h). A similar vertical pattern has been shown by Iwao and Takahashi (2008), who found that quasi-stationary

Rossby waves propagating on waveguides along the Asian jet and over northern Eurasia are responsible for a dominant seesaw pattern in summertime precipitation between northeast Asia and Siberia.

In summary, the structure and evolution of the 7–20-day ETPSR ISO during the dry phase characterizes as a vertical dipole pattern of geopotential height with a positive center over the eastern TP and a negative center over the western TP located in the upper troposphere, which is accompanied by a negative temperature anomaly (Fig. 5a). The wet phase presents the opposite characteristics of the dry phase (cf. Figs. 5e and 5a). The transitions between dry and wet phases (Figs. 4b–d,f–h) during an ETPSR ISO are related to the eastward-propagating wave train extending from the eastern Atlantic to the western TP.

4. Teleconnection between the summer Eurasian wave train and the ETPSR ISO

The above phase composite analysis suggests that the evolution of the ETPSR ISO is related to the intraseasonal variability of a wave train over the eastern Atlantic and Eurasia. Previous studies showed that a teleconnection pattern in the upper troposphere emerges from North Africa to East Asia along the westerly jet in the middle latitudes (Lu et al. 2002); i.e., “the Silk Road pattern” (Enomoto et al. 2003). This teleconnection pattern is also a possible linkage of the East Asia summer monsoon to the Indian monsoon (Ding and Wang 2007), and even to subtropical heating anomalies over the Atlantic. Terao (1998, 1999) showed that quasi-stationary Rossby waves occur on the Asian subtropical jet during the boreal summer, with spectral peaks at 14 and 30–45 days. This raises the question of whether the Rossby wave train suggested by previous studies has significant intraseasonal fluctuations with a similar period to the ETPSR ISO. If so, what is the teleconnection process between them? We will explore this possible teleconnection below.

Horel (1981) inferred several properties of the rotated empirical orthogonal functions (REOF) and pointed out that it will exactly reproduce the variability explained by the principal components, but is less dependent on the domain of the analysis. As a result, REOF analysis via an anomaly covariance matrix was used to identify the dominant patterns in daily geopotential height at 200 hPa for the 33 summers (1979–2011) within the domain 20°–70°N, 30°W–150°E. To lessen the influence of high-latitude grid points, the anomalies were area-weighted prior to the REOF analysis by multiplying by a matrix containing the square root of the cosine of the specific latitudes. We also checked the results generated by EOF analysis,

which were similar to those obtained from the REOF analysis.

Figure 6 shows the first three leading REOF patterns of the geopotential height field, which explain 10.4%, 9.5%, and 8.5% of the total variance, respectively. The first REOF pattern (Fig. 6a) displays a southeastward-propagating wave train, starting from a strong positive center over the northern Atlantic and others over central Asia, the TP, and southern China, with elongated negative loading in between. The second REOF (Fig. 6b) shows an obvious wave train at high latitudes, extending from the anomalous center located in the northern Atlantic, passing through Europe and northern Russia and down to East Asia. Seo et al. (2012) found that this kind of Rossby wave may have been the cause of the extraordinary East Asian summer monsoon event in July 2011. The third REOF (Fig. 6c) presents similar features to the second, except that the wave train starts from the positive loading in the eastern Atlantic. It consists of three anomalous highs over the eastern Atlantic, northern Europe, and the central-eastern TP and Far East, and two anomalous lows over the northern Atlantic and eastern Siberia. All three REOF patterns affect the upper-level circulation over the ETP, further influencing the rainfall variability there.

The dominant period of the wave train oscillation was determined from the power spectral analysis of the three leading REOF principal component time series (PC1–3; right panels in Fig. 6). The spectrum of PC1 reaches its variance peak at 19 days, whereas the peaks of PC2 and PC3 are at 30 days. Although the peak period differs from PC1 to PC2/PC3, a common period of 7–30 days for the three PCs passes the 95% confidence level against a red noise process. The lead–lag correlations between the three PCs suggest that the three leading REOFs may be considered as different propagating phases of the summer Eurasian wave train, which together account for about 28.4% of the subseasonal variance (figure not shown). According to the definition of the time scale of teleconnection, patterns can be classified into two types: intermediate and low frequency (Blackmon et al. 1984a,b; Lu et al. 2002), and the wave train suggested by the three leading REOF patterns belongs to the intermediate time scale teleconnection. This kind of teleconnection can be interpreted in terms of two-dimensional Rossby wave dispersion, with a predominance of southward dispersion from middle latitudes into the tropics (Blackmon et al. 1984b).

Observing that the evolution of the 7–20-day ISO of ETPSR is associated with the mainly eastward and southeastward propagation of a wave train (Fig. 4), to further investigate the teleconnection between the Rossby wave train and ETPSR on the 7–20-day time scale we performed a lead–lag regression analysis of

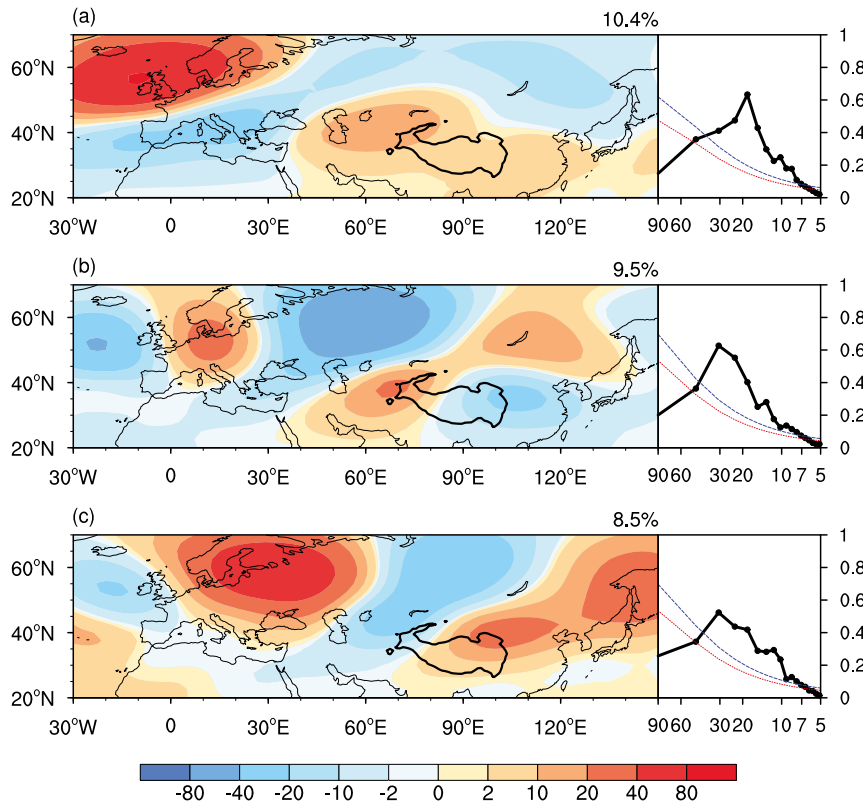


FIG. 6. (left) First three REOF modes for 33-summer daily geopotential height at 200 hPa and (right) averaged power spectra of the corresponding PCs. The TP with terrain above 3000 m is outlined by the solid black curve in the left panels. The red dotted and blue dashed lines in the right panels represent the Markov red noise spectrum and a 95% confidence level, respectively.

ETPSRI with respect to the standardized first three REOF PCs between June and August over the period 1979–2011 (Fig. 7). On the 7–20-day time scale, the anomalies of ETPSRI simultaneously regressed upon PC1/PC2 (PC3) are significantly positive (negative) at day 0. It is evident that the ETPSRI maximum leads PC2 (PC3) by 6 (5) days, and the ETPSRI minimum leads PC1 by 6 days. The next maxima of rainfall anomaly lag PC2 and PC3 by 2 and 4 days, respectively, and the rainfall minimum lags PC1 by 5 days. This indicates that there is an obvious lead–lag relationship between ETPSR and different propagating phases of the summer Eurasian wave train over the 7–20-day time scale. This also supports our view that the wave train over the eastern Atlantic and Eurasian continent has important impacts on the intraseasonal variability of ETPSR.

5. Impact of fluctuations over the eastern Atlantic on ETPSR

The results presented in sections 3 and 4 suggest that the fluctuations over the eastern Atlantic in the 20°–50°N

latitude band are vital to our understanding of the propagation of the intraseasonal midlatitude wave train related to the 7–20-day ETPSR ISO (Figs. 4–6). In this section, we study further the impact of fluctuations over the eastern Atlantic on ETPSR.

Figure 8a shows the 7–20-day-filtered pressure vertical velocity at 500 hPa associated with the ETPSR ISO. Note that negative (positive) values of pressure vertical velocity represent ascending (descending) motion. A strong center of ascending motion is located over the ETP, which corresponds to wet phases of the ETPSR ISO. There is a statistically significant wave train, which consists of a series of alternating positive and negative centers of vertical velocity, extending from the eastern Atlantic (positive) to southern China (positive) via the Alps (negative), Black Sea (positive), Caspian Sea (negative), western TP (positive), and ETP (negative). This is consistent with the upper-level circulation and vertical structure of the wave train shown in section 3 (Fig. 8a vs Figs. 4 and 5). We assume that the 500-hPa pressure vertical velocity represents the amplitude of the fluctuation. Thus, the vertical velocity averaged over

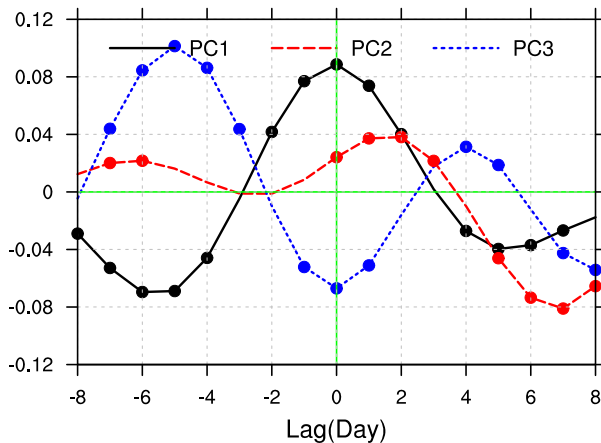


FIG. 7. Anomalies of the 7–20-day-filtered ETPSRI (mm day^{-1}) obtained by lead–lag regression onto the standardized first three PCs for the 33 summers between 1979 and 2011, respectively. Marked points denote that the corresponding correlation coefficients are significant at the 95% confidence level. The negative (positive) numbers along the horizontal axis denote the days when PCs lag (lead) rainfall over the ETP.

the eastern Atlantic region (30° – 45°N , 5° – 20°W ; red rectangle in Fig. 8) at 500 hPa is defined as the eastern Atlantic vertical velocity index (EAVVI) for simplicity. The spatial pattern of the 7–20-day-filtered vertical velocity regressed upon the EAVVI at 500 hPa (Fig. 8b) also displays a similar significant wave train to that in Fig. 8a, with the negative center over the ETP. This suggests that the fluctuation over the eastern Atlantic may link to the propagation of the wave train associated with the ETPSR ISO. The fluctuation is also closely associated with the North Atlantic Oscillation (NAO). Note that the wave train structure remains clear over the area west of the EAVVI region and the signals are very obvious from high latitudes (Fig. 9b). This indicates that the fluctuation over the eastern Atlantic may be related to the variability of the Arctic sea ice, because concentrations of sea ice are correlated with the NAO (Deser et al. 2000; Partington et al. 2003).

To further explore the upper-level circulation over the TP region, we compared the regressed anomalies of the 7–20-day-filtered geopotential height and winds at 200 hPa with respect to the ETPSRI with the same fields after the eastern Atlantic fluctuation effect was removed (Fig. 9). It is evident that the patterns of geopotential height and winds over the TP and its surrounding regions with respect to the ETPSRI (Fig. 9a) are similar to those of the composite anomalies during the wet phase (Fig. 4e). However, when we removed the effect of the eastern Atlantic fluctuation by subtracting the linear component regressed upon EAVVI, the magnitudes of the geopotential height centers and winds were reduced

(Fig. 9b). These results again support the potential influence of the eastern Atlantic fluctuation on ETPSR. As the zonal gradients of the basic flow are particularly strong in the jet stream exit region, the fluctuation in the eastern Atlantic, which is presumably excited by the upstream extratropical forcing along the Atlantic jet stream, might be considered to be the origin of the midlatitude wave train (Simmons et al. 1983; Hoskins et al. 1983; Ding and Wang 2007). This is consistent with our results showing that the eastern Atlantic fluctuation plays an important role in the propagation of the intraseasonal wave train that is closely related to the ETPSR ISO.

To further confirm the role of the eastern Atlantic fluctuation in the generation of the intraseasonal wave train in the midlatitudes, we performed a control run (CON) and a sensitivity experiment (SEN) using the AGCM described in section 2. Both experiments were integrated for 10 years. The settings for SEN were the same as in CON, but with the addition of an idealized three-dimensional heating over the eastern Atlantic region from 1 June to 31 August in each integration year. The vertical structure of the heating followed a latent heating profile and the intensity of the heat was calculated from the model's climate-mean latent heating in monsoon regions (Fig. 10a). The horizontal distribution of the heating was a circle with its center located at 35°N , 20°W , and with a 15° radius (Fig. 10b).

To better compare the model results with the observed features, we conducted a composite analysis of the circulation pattern in the observations (Fig. 11a) and of the difference field (SEN minus CON; Fig. 11b). The criterion used for the composite analysis was that the geopotential height averaged over the ETP (25° – 40°N , 85° – 105°E) was greater than the threshold of 1.5 standard deviations. If the difference field (SEN minus CON) shows an intraseasonal wave train comparable with that observed, it indicates that the eastern Atlantic fluctuation is able to excite a midlatitude wave train. A wave train is observed in Fig. 11a with several obvious centers of geopotential height alternately located over the eastern Atlantic (negative), northeastern Atlantic (positive), western Europe (negative), eastern Europe (positive), western TP (negative), and ETP (positive), accompanied by a corresponding anticyclonic/cyclonic circulation. As shown in Fig. 11b, the simulated pattern of the wave train in the upper-level troposphere is fairly similar to that in the observations. As a result, the sensitivity experiment with the additional idealized three-dimensional heating over the eastern Atlantic region further confirms that fluctuations in the eastern Atlantic may be considered to be a key factor that influences the propagation of the intraseasonal wave train in the

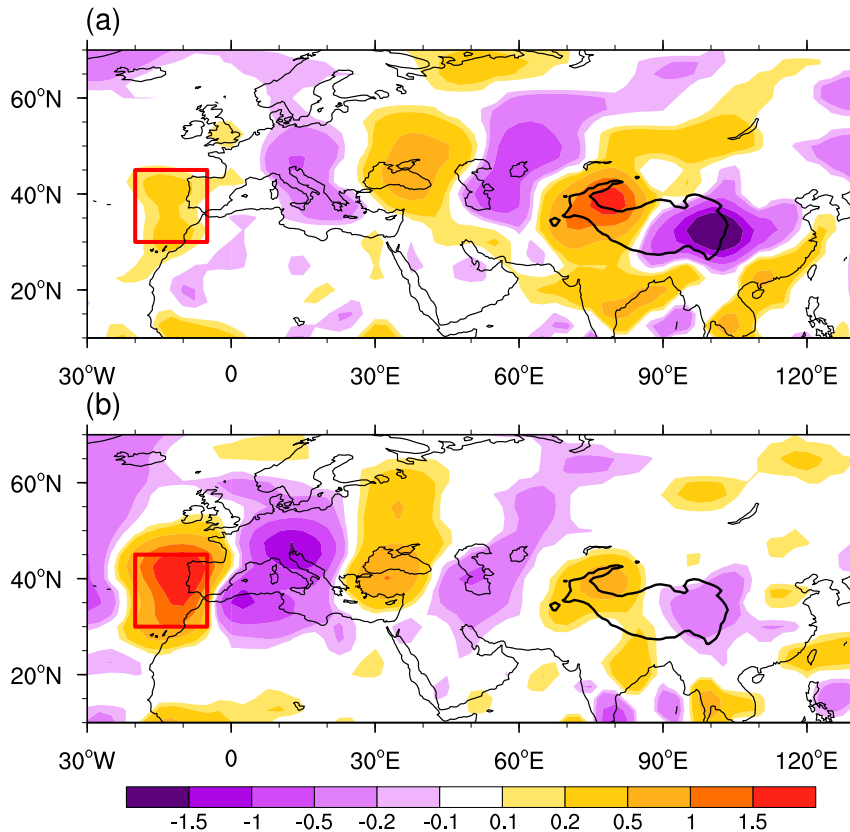


FIG. 8. Regressed anomalies of 7–20-day-filtered pressure vertical velocity (Pa s^{-1}) at 500 hPa with respect to (a) ETPSRI and (b) EAVVI. The area over which EAVVI is defined is marked by the red rectangle. Only the values of pressure vertical velocity that are statistically significant at the 95% confidence level are plotted. The TP with terrain above 3000 m is outlined by the solid black curve.

midlatitudes, which in turn influences the upper-level circulation over the ETP and southern China. The eastward/southeastward propagation of this wave train partly determines the intraseasonal cycle of the ETPSR ISO and southern China's summer rainfall ISO.

6. Summary and discussion

In the present study, the structure and propagation characteristics of the dominant intraseasonal oscillation (ISO) controlling summer rainfall over the eastern Tibetan Plateau (ETP) were examined based on rain gauge data and NCEP–DOE reanalysis products for the period 1979–2011. In addition, we also investigated the link between the dominant ISO and the summer Eurasian wave train, as well as the impact of fluctuations over the eastern Atlantic on ETP summer rainfall (ETPSR).

Both power spectrum and wavelet spectrum analysis were applied to ETPSR index (ETPSRI) to determine the dominant ISO periods. Our results showed that an oscillation of ETPSR with a statistically significant period

of 7–20 days exists for most summers between 1979 and 2011, although the percentage variance of the 7–20-day oscillation varies with the year. Composite results revealed that the evolution of the 7–20-day ETPSR ISO is closely related to the mainly eastward and southeastward propagation of a wave train characterized by large anomalous anticyclonic and cyclonic centers alternating along the pathway from the eastern Atlantic to southern China via the TP in the upper-level troposphere, with strong divergence or convergence in between. This corresponds closely to the evolution of the phase-independent wave-activity \mathbf{W} , which implies an eastward/southeastward energy propagation of the ISO.

The vertical structure of the ETPSR ISO during the dry phase characterizes as a vertical dipole pattern of geopotential height with a positive center over the eastern TP and a negative center over the western TP located in the upper troposphere. The wet phase presents the opposite characteristics to those of the dry phase. The transition between dry and wet phases during an ETPSR ISO is related to the eastward-propagating wave train extending

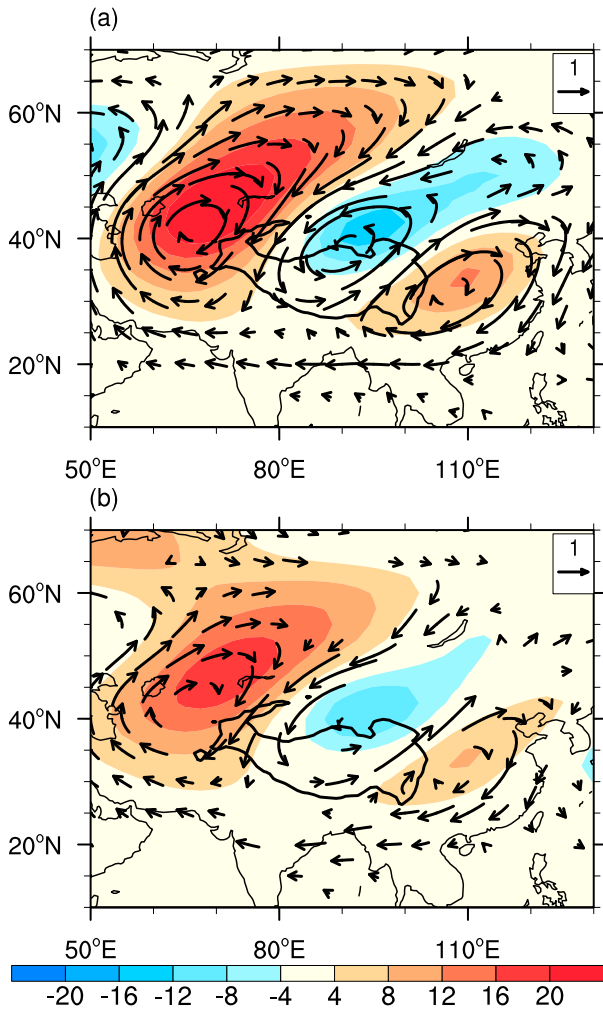


FIG. 9. (a) Regressed anomalies of 7–20-day-filtered geopotential height (gpm) and winds (m s^{-1}) at 200 hPa with respect to ETPSRI. (b) As in (a), but without the eastern Atlantic fluctuation effect removed by subtracting the linear component regressed against EAVVI. Only values that are statistically significant at the 95% confidence level are plotted. The TP with terrain above 3000 m is outlined by the solid black curve.

from the eastern Atlantic to the western TP. At first, a weak negative geopotential height center with ascending motion develops below 300 hPa in the eastern Atlantic during the dry phase. Then, it strengthens and induces a positive geopotential height center appearing at 150 hPa to its east. The process of continuous strengthening and slow eastward movement of the anomalous geopotential height centers eventually influences the vertical structure of the ISO around and on the TP.

The picture emerging from our REOF analysis, which was applied to the daily 200-hPa geopotential height field, demonstrates that the REOF patterns represent the different phases of an obvious wave train extending

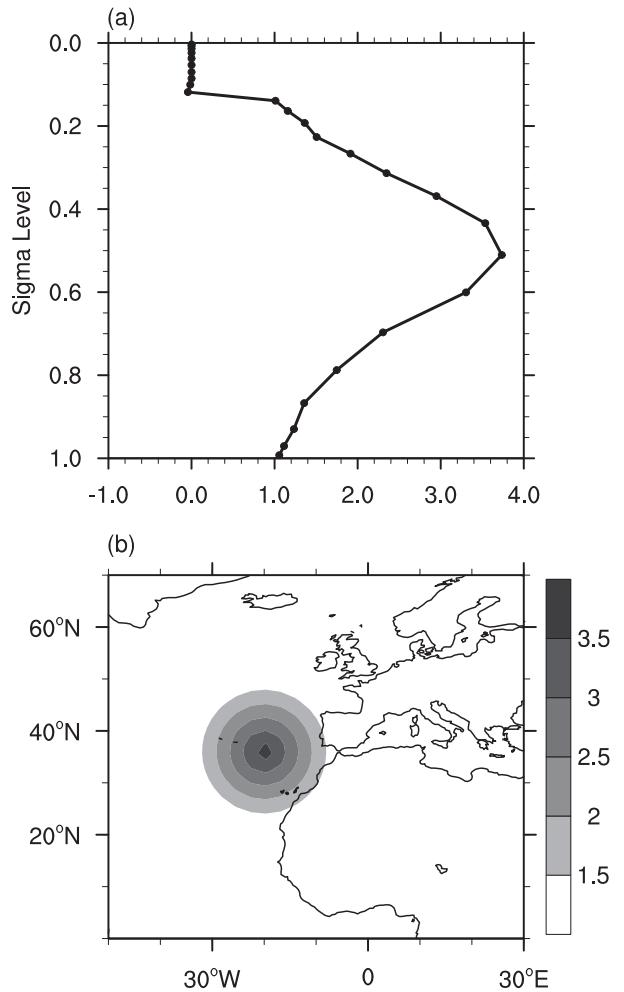


FIG. 10. (a) Latent heating profile and (b) horizontal distribution of the idealized heating (K day^{-1}) in the SEN experiment design.

from the eastern Atlantic to East Asia that impacts the upper-level circulation over the ETP. All three corresponding PCs have a 7–30-day common period that is significant at the 95% level. The lead-lag regression between the ETPSRI and the first three REOF PCs also supports our view that the wave train over the eastern Atlantic and Eurasian continent has important impacts on the intraseasonal variability of ETPSR.

The patterns of vertical velocity in the middle-layer troposphere regressed upon the ETPSRI also show a statistically significant wave train extending from the eastern Atlantic to southern China via the Alps, the Black Sea, the Caspian Sea, and the TP. The regression analysis of vertical velocity at 500 hPa with respect to EAVVI suggests that the fluctuation over the eastern Atlantic is closely related to the propagation of the wave train associated with the ETPSR ISO. If we then remove the effect of this eastern Atlantic fluctuation,

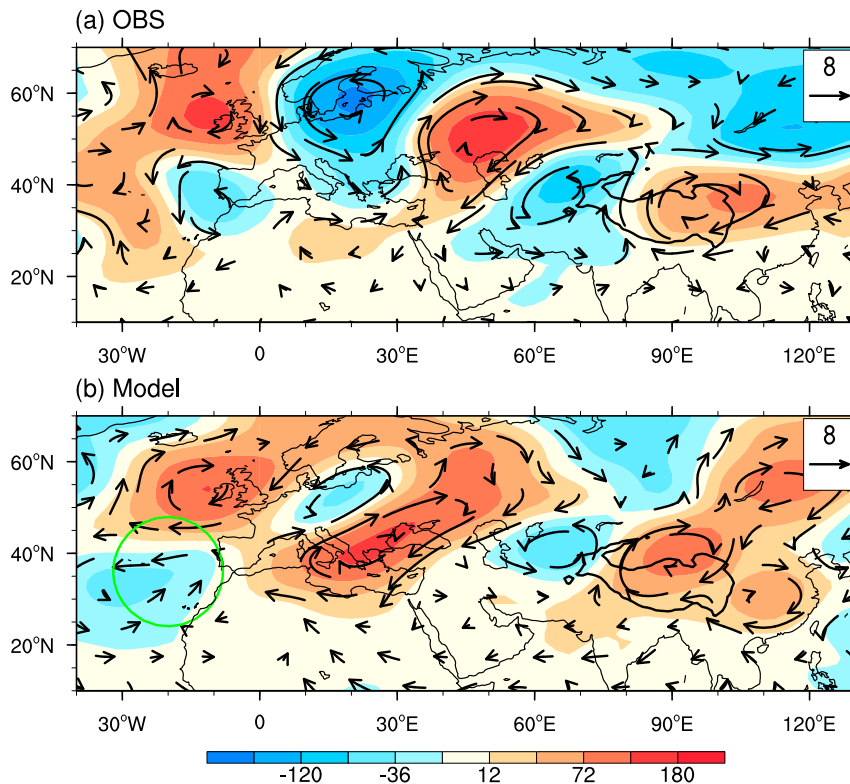


FIG. 11. Composite anomalies of the 7–20-day-filtered geopotential height (shading; gpm) and winds (vectors; m s^{-1}) at 200 hPa during JJA for (a) the observations and (b) SEN minus CON when the area-averaged geopotential height over the ETP is greater than the threshold of 1.5 standard deviations. The green solid curve represents the 1.5 K day^{-1} contour of the idealized heating. The TP with terrain above 3000 m is outlined by the solid black curve.

the magnitudes of the geopotential height centers and winds in the upper-level troposphere decrease, which again supports the potential role of the eastern Atlantic fluctuations in influencing ETPSR. We also conducted a sensitivity experiment with an additional idealized three-dimensional heating over the eastern Atlantic region. Comparison with the control run confirmed that the fluctuation in the eastern Atlantic may be considered to be the key factor for the propagation of the midlatitude intraseasonal wave train that influences the upper-level circulation and rainfall variability over the ETP and southern China. The eastern Atlantic fluctuations may result from upstream tropical or extratropical forcing along the Atlantic jet stream. According to the theory of Simmons et al. (1983), the disturbances in the jet stream exit region could be excited by efficient kinetic energy extraction from the basic state through barotropic energy conversions; this was also proposed by Ding and Wang (2007).

In addition to pointing out the relationship between low-frequency transients and barotropic instability, Simmons et al. (1983) demonstrated that the baroclinic

waves influence the time evolution of the low-frequency transients in complicated ways and that the picture is confused further by the interactions between the low-frequency transients and the orographic forcing. It is well known that the TP has highly elevated terrain and is a very strong heat source in summer. This may indicate that both thermal and mechanical forcing by the TP will modulate the wave train evolution during its propagation. Thus, the summer Eurasian wave train is not the only factor that determines the evolution of the ETPSR ISO. The effect of the TP itself on the intraseasonal variability of ETPSR needs further analysis.

As we have shown, the summer Eurasian wave train has a significant impact on rainfall variability over the TP, and also influences the Indian summer monsoon (Ding and Wang 2007) and northern China (Lu et al. 2002). This wave train links the upper-level circulation of the Indian summer monsoon to the East Asia summer monsoon. What then are the physical processes of interaction between the ISOs in the TP, South Asia, and East Asia? We will examine them in a future study.

Acknowledgments. The authors appreciate the editor and three anonymous reviewers for their comments. This work was jointly supported by the National Key Basic Research Program of China (2015CB453202 and 2014CB953902), the National Natural Science Foundation of China (41305065 and 91337216), and the Open Project of the Key Laboratory of Meteorological Disaster of the Ministry of Education (KLME1503). Wenting Hu received funding support for a visiting scholar through the China Scholarship Council for conducting research at CSIRO.

REFERENCES

- Annamalai, H., and J. M. Slingo, 2001: Active/break cycles: Diagnosis of the intraseasonal variability of the Asian summer monsoon. *Climate Dyn.*, **18**, 85–102, doi:10.1007/s003820100161.
- Bao, Q., and Coauthors, 2013: The Flexible Global Ocean–Atmosphere–Land system model, spectral version 2: FGOALS-s2. *Adv. Atmos. Sci.*, **30**, 561–576, doi:10.1007/s00376-012-2113-9.
- Blackmon, M. L., Y.-H. Lee, and J. M. Wallace, 1984a: Horizontal structure of 500-mb height fluctuations with long, intermediate and short timescales. *J. Atmos. Sci.*, **41**, 961–980, doi:10.1175/1520-0469(1984)041<0961:HSOMHF>2.0.CO;2.
- , —, —, and H.-H. Hsu, 1984b: Time variation of 500-mb height fluctuations with long, intermediate, and short time scales as deduced from lag-correlation statistics. *J. Atmos. Sci.*, **41**, 981–991, doi:10.1175/1520-0469(1984)041<0981:TVOMHF>2.0.CO;2.
- Dai, F. S., R. C. Yu, X. H. Zhang, and Y. Q. Yu, 2004: A statistical low-level cloud scheme and its tentative application in a general circulation model (in Chinese). *Acta Meteor. Sin.*, **62**, 385–394.
- Dee, D. P., and Coauthors, 2011: The ERA-Interim reanalysis: Configuration and performance of the data assimilation system. *Quart. J. Roy. Meteor. Soc.*, **137**, 553–597, doi:10.1002/qj.828.
- Deser, C., J. E. Walsh, and M. S. Timlin, 2000: Arctic sea ice variability in the context of recent atmospheric circulation trends. *J. Climate*, **13**, 617–633, doi:10.1175/1520-0442(2000)013<0617:ASIVIT>2.0.CO;2.
- Ding, Q., and B. Wang, 2007: Intraseasonal teleconnection between the summer Eurasian wave train and the Indian monsoon. *J. Climate*, **20**, 3751–3767, doi:10.1175/JCLI4221.1.
- Duchon, C. E., 1979: Lanczos filtering in one and two dimensions. *J. Appl. Meteor.*, **18**, 1016–1022, doi:10.1175/1520-0450(1979)018<1016:LFOAT>2.0.CO;2.
- Edwards, J. M., and A. Slingo, 1996: Studies with a flexible new radiation code. I: Choosing a configuration for a large-scale model. *Quart. J. Roy. Meteor. Soc.*, **122**, 689–719, doi:10.1002/qj.49712253107.
- Enomoto, T., B. J. Hoskins, and Y. Matsuda, 2003: The formation mechanism of the Bonin high in August. *J. Meteor. Soc. Japan*, **129**, 157–178, doi:10.1256/qj.01.211.
- Fujinami, H., and T. Yasunari, 2001: The seasonal and intraseasonal variability of diurnal cloud activity over the Tibetan Plateau. *J. Meteor. Soc. Japan*, **79**, 1207–1227, doi:10.2151/jmsj.79.1207.
- , and —, 2004: Submonthly variability of convection and circulation over and around the Tibetan Plateau during the boreal summer. *J. Meteor. Soc. Japan*, **82**, 1545–1564, doi:10.2151/jmsj.82.1545.
- , and —, 2009: The effects of midlatitude waves over and around the Tibetan Plateau on submonthly variability of the East Asian summer monsoon. *Mon. Wea. Rev.*, **137**, 2286–2304, doi:10.1175/2009MWR2826.1.
- Gilman, D. L., F. J. Fuglister, and J. M. Mitchell Jr., 1963: On the power spectrum of “red noise.” *J. Atmos. Sci.*, **20**, 182–184, doi:10.1175/1520-0469(1963)020<0182:OTPSON>2.0.CO;2.
- Goswami, B. N., 2005: South Asian summer monsoon. *Intraseasonal Variability of the Atmosphere–Ocean Climate System*, W. K. M. Lau and D. E. Waliser, Eds., Springer, 19–62.
- Holtstlag, A. A. M., and B. A. Boville, 1993: Local versus non-local boundary layer diffusion in a global climate model. *J. Climate*, **6**, 1825–1842, doi:10.1175/1520-0442(1993)006<1825:LVNBLD>2.0.CO;2.
- Horel, J. D., 1981: A rotated principal component analysis of the interannual variability of the Northern Hemisphere 500-mb height field. *Mon. Wea. Rev.*, **109**, 2080–2092, doi:10.1175/1520-0493(1981)109<2080:ARPCAO>2.0.CO;2.
- Horinouchi, T., 2014: Influence of upper tropospheric disturbances on the synoptic variability of precipitation and moisture transport over summertime East Asia and the northwestern Pacific. *J. Meteor. Soc. Japan*, **92**, 519–541, doi:10.2151/jmsj.2014-602.
- Hoskins, B. J., I. N. James, and G. H. White, 1983: The shape, propagation and mean-flow interaction of large-scale weather systems. *J. Atmos. Sci.*, **40**, 1595–1612, doi:10.1175/1520-0469(1983)040<1595:TSPAMF>2.0.CO;2.
- Hu, W., A. Duan, and G. Wu, 2015: Impact of subdaily air–sea interaction on simulating intraseasonal oscillations over the tropical Asian monsoon region. *J. Climate*, **28**, 1057–1073, doi:10.1175/JCLI-D-14-00407.1.
- Iwao, K., and M. Takahashi, 2008: A precipitation seesaw mode between northeast Asia and Siberia in summer caused by Rossby waves over the Eurasian continent. *J. Climate*, **21**, 2401–2419, doi:10.1175/2007JCLI1949.1.
- Jiang, X., T. Li, and B. Wang, 2004: Structures and mechanisms of the northward propagating boreal summer intraseasonal oscillation. *J. Climate*, **17**, 1022–1039, doi:10.1175/1520-0442(2004)017<1022:SAMOTN>2.0.CO;2.
- Kanamitsu, M., W. Ebisuzaki, J. Woollen, S.-K. Yang, J. J. Hnilo, M. Fiorino, and G. L. Potter, 2002: NCEP–DOE AMIP-II Reanalysis (R-2). *Bull. Amer. Meteor. Soc.*, **83**, 1631–1643, doi:10.1175/BAMS-83-11-1631.
- Lawrence, D. M., and P. J. Webster, 2002: The boreal summer intraseasonal oscillation: Relationship between northward and eastward movement of convection. *J. Atmos. Sci.*, **59**, 1593–1606, doi:10.1175/1520-0469(2002)059<1593:TBSIOR>2.0.CO;2.
- Lu, R.-Y., J.-H. Oh, and B.-J. Kim, 2002: A teleconnection pattern in upper-level meridional wind over the North African and Eurasian continent in summer. *Tellus*, **54A**, 44–55, doi:10.1034/j.1600-0870.2002.00248.x.
- Madden, R. A., and P. R. Julian, 1971: Detection of a 40–50 day oscillation in the zonal wind in the tropical Pacific. *J. Atmos. Sci.*, **28**, 702–708, doi:10.1175/1520-0469(1971)028<0702:DOADOI>2.0.CO;2.
- , and —, 1972: Description of global-scale circulation cells in the tropics with a 40–50 day period. *J. Atmos. Sci.*, **29**, 1109–1123, doi:10.1175/1520-0469(1972)029<1109:DOGSCC>2.0.CO;2.
- Mao, J. Y., and J. C. L. Chan, 2005: Intraseasonal variability of the South China Sea summer monsoon. *J. Climate*, **18**, 2388–2402, doi:10.1175/JCLI3395.1.
- Murakami, T., 1981: Orographic influence of the Tibetan Plateau on the Asiatic winter monsoon circulation. Part IV. Long-period oscillations. *J. Meteor. Soc. Japan*, **59**, 201–219.

- Naoe, H., and Y. Matsuda, 1998: Rossby wave propagation and nonlinear effects in zonally-varying basic flows. *J. Meteor. Soc. Japan*, **76**, 385–402.
- , —, and H. Nakamura, 1997: Rossby wave propagation in idealized and realistic zonally varying flows. *J. Meteor. Soc. Japan*, **75**, 687–700.
- Oleson, K. W., and Coauthors, 2004: Technical description of the Community Land Model (CLM). NCAR Tech. Note NCAR/TN-461+STR, 173 pp., doi:10.5065/D6N877R0.
- Pan, W., J. Mao, and G. Wu, 2013: Characteristics and mechanism of the 10–20-day oscillation of spring rainfall over southern China. *J. Climate*, **26**, 5072–5087, doi:10.1175/JCLI-D-12-00618.1.
- Park, H.-S., B. R. Lintner, W. R. Boos, and K.-H. Seo, 2015: The effect of midlatitude transient eddies on monsoonal southerlies over eastern China. *J. Climate*, **28**, 8450–8465, doi:10.1175/JCLI-D-15-0133.1.
- Partington, K., T. Flynn, D. Lamb, C. Bertoia, and K. Dedrick, 2003: Late twentieth century Northern Hemisphere sea-ice record from U.S. National Ice Center ice charts. *J. Geophys. Res.*, **108**, 3343, doi:10.1029/2002JC001623.
- Plumb, R. A., 1985: On the three-dimensional propagation of stationary waves. *J. Atmos. Sci.*, **42**, 217–229, doi:10.1175/1520-0469(1985)042<0217:OTDPO>2.0.CO;2.
- Seo, K.-H., J.-H. Son, S.-E. Lee, T. Tomita, and H.-S. Park, 2012: Mechanisms of an extraordinary East Asian summer monsoon event in July 2011. *Geophys. Res. Lett.*, **39**, L05704, doi:10.1029/2011GL050378.
- Simmons, A. J., J. M. Wallace, and G. W. Branstator, 1983: Barotropic wave propagation and instability, and atmospheric teleconnection patterns. *J. Atmos. Sci.*, **40**, 1363–1392, doi:10.1175/1520-0469(1983)040<1363:BWPAlA>2.0.CO;2.
- Slingo, J. M., 1980: A cloud parameterization scheme derived from GATE data for use with a numerical model. *Quart. J. Roy. Meteor. Soc.*, **106**, 747–770, doi:10.1002/qj.49710645008.
- , 1989: A GCM parameterization for the shortwave radiative properties of water clouds. *J. Atmos. Sci.*, **46**, 1419–1427, doi:10.1175/1520-0469(1989)046<1419:AGPFTS>2.0.CO;2.
- Sun, Z., 2011: Improving transmission calculations for the Edwards–Slingo radiation scheme using a correlated- k distribution method. *Quart. J. Roy. Meteor. Soc.*, **137**, 2138–2148, doi:10.1002/qj.880.
- Takaya, K., and H. Nakamura, 2001: A formulation of a phase independent wave-activity flux for stationary and migratory quasigeostrophic eddies on a zonally varying basic flow. *J. Atmos. Sci.*, **58**, 608–627, doi:10.1175/1520-0469(2001)058<0608:AFOAPI>2.0.CO;2.
- Terao, T., 1998: Barotropic disturbances on intraseasonal time scales observed in the midlatitudes over the Eurasian Continent during the northern summer. *J. Meteor. Soc. Japan*, **76**, 419–436.
- , 1999: The zonal wavelength of the quasistationary Rossby waves trapped in the westerly jet. *J. Meteor. Soc. Japan*, **77**, 687–699.
- Tiedtke, M., 1989: A comprehensive mass flux scheme for cumulus parameterization in large-scale models. *Mon. Wea. Rev.*, **117**, 1779–1800, doi:10.1175/1520-0493(1989)117<1779:ACMFSF>2.0.CO;2.
- Torrence, C., and G. P. Compo, 1998: A practical guide to wavelet analysis. *Bull. Amer. Meteor. Soc.*, **79**, 61–78, doi:10.1175/1520-0477(1998)079<0061:APGTWA>2.0.CO;2.
- Waliser, D. E., 2005: Predictability and forecasting. *Intraseasonal Variability of the Atmosphere–Ocean Climate System*, W. K. M. Lau and D. E. Waliser, Eds., Springer, 389–424.
- , 2006: Intraseasonal variability. *The Asian Monsoon*, B. Wang, Ed., Springer, 203–258.
- Wu, G., H. Liu, Y. Zhao, and W. Li, 1996: A nine-layer atmospheric general circulation model and its performance. *Adv. Atmos. Sci.*, **13**, 1–18, doi:10.1007/BF02657024.
- Yang, J., B. Wang, and B. Wang, 2008: Anti-correlated intensity change of the quasi-biweekly and 30–50-day oscillations over the South China Sea. *Geophys. Res. Lett.*, **35**, L16702, doi:10.1029/2008GL034449.
- , —, —, and Q. Bao, 2010: Biweekly and 21–30-day variations of the subtropical summer monsoon rainfall over the lower reach of the Yangtze River basin. *J. Climate*, **23**, 1146–1160, doi:10.1175/2009JCLI3005.1.
- , Q. Bao, B. Wang, D.-Y. Gong, H. He, and M.-N. Gao, 2014: Distinct quasi-biweekly variations of the subtropical East Asian monsoon during early and late summers. *Climate Dyn.*, **42**, 1469–1486, doi:10.1007/s00382-013-1728-6.
- Yasunari, T., 1979: Cloudiness fluctuations associated with the Northern Hemisphere summer monsoon. *J. Meteor. Soc. Japan*, **57**, 227–242.
- , 1980: A quasi-stationary appearance of 30 to 40 day period in the cloudiness fluctuations during the summer monsoon over India. *J. Meteor. Soc. Japan*, **58**, 225–229.
- , 1981: Structure of an Indian summer monsoon system with around 40-day period. *J. Meteor. Soc. Japan*, **59**, 336–354.